

Contents lists available at ScienceDirect

Intermetallics

journal homepage: www.elsevier.com/locate/intermet





Structural and magnetic transitions of CoFeMnNiAl high-entropy alloys caused by composition and annealing

Tingting Zuo ^{a,b,c}, Yongqiang Cheng ^d, Peiyong Chen ^c, Zhaoshun Gao ^a, Yong Zhang ^{b,*}, Peter K. Liaw ^{c,**}

- ^a Interdisciplinary Research Center, Institute of Electrical Engineering of Chinese Academy of Sciences, Beijing, 100190, China
- b State Key Laboratory for Advanced Metals and Materials, University of Science and Technology Beijing, Beijing, 100083, China
- E Department of Materials Science and Engineering, The University of Tennessee, Knoxville, TN, 37996, USA
- ^d Chemical and Engineering Materials Division, Oak Ridge National Laboratory, Oak Ridge, TN, 37831, USA

ARTICLE INFO

Keywords: High-entropy alloy Annealing Phase structure Magnetic property Ab initio calculation

ABSTRACT

Tailoring magnetic behavior by composition and annealing is an effective way. The phase transition from the face-centered-cubic (FCC) to B2 structure influenced by the Al content on the CoFeMnNiAl $_x$ alloys leads to the enhanced magnetization. However, the excessive Al addition in the B2-structured alloys impairs the magnetization. The phase transformation caused by annealing also indicates that the saturation magnetization of the alloy depends on the volume fraction of the B2 phase, and a higher content of the B2 phase is beneficial to the large saturation magnetization. *Ab initio* calculations are used to explain the magnetic behavior of the present HEAs and the effects of phase structures on magnetic characteristics. The phase stability of the CoFeMnNiAl $_x$ alloy is thoroughly studied by both the existing phase-formation empirical criteria and annealing. The existing empirical criteria used to predict the phase formation are not universal. However, combining the ΔH_{mix} - δ relation and the ϕ value, whether the single disordered solid-solution phase is formed can be preliminarily predicted.

1. Introduction

The quickly-developed high-entropy alloy (HEA) opens a new way for alloy design, which arouses extensive attentions in the various countries [1-9]. Different from the conventional alloy, the HEA is characterized by its special compositions containing at least five elements in equal or near-equal molar ratios. This design concept leads to the high configurational entropy of mixing, which suppresses the formation of intermetallic compounds and promotes the formation of the solid-solution phases [10]. Owing to the unique solid-solution structures, HEAs may possess excellent properties, such as high strength [11, 12], great fracture toughness and fatigue resistance [13-15], good room-temperature ductility [16], high thermal stability and corrosion resistance [17,18], etc. In addition to the extraordinary mechanical properties, HEAs have also been suggested to be used as soft magnetic materials [19-21], since HEAs can simultaneously possess the high saturation magnetization and good balance between strength and ductility by carefully designing the composition and phase structure [19,

20]. In our previous study, we designed a novel CoFeMnNiAl alloy and found the equal-atomic percentage of the Al addition into the face-centered-cubic (FCC)-structured CoFeMnNi alloy can significantly enhance the magnetization by tailoring the phase structure [22]. However, the effect of the aluminum content on the microstructure and magnetic transition remains unclear. Whether the Al addition will always increase the magnetization of materials remains to be further explored. Besides, the as-cast CoFeMnNiAl alloy seems to have an unstable phase structure, and recent studies also found that some HEAs do not maintain their single-phase structure during the heat treatment [23]. Annealing as an effective mean is often used to tailor the structures and properties of HEA alloys. In this paper, aiming to deeply investigate the phase stability and find the relationship between the magnetic property and phase structure, the CoFeMnNiAl_x (x = 0.25, 0.5, 0.75, 1.0, 1.25,1.5, and 2.0) alloys are designed. The role of the Al addition on the phase transformation and magnetic transition is explored. Long-time annealing was conducted to study the phase stability. Ab initio calculations were used to explain the relationship between phase structures and

^{*} Corresponding author. Department of Materials Science and Engineering, The University of Tennessee, Knoxville, TN, 37996, USA.

^{**} Corresponding author. State Key Laboratory for Advanced Metals and Materials, University of Science and Technology Beijing, Beijing, 100083, China. E-mail addresses: zuotingting@mail.iee.ac.cn (T. Zuo), drzhangy@ustb.edu.cn (Y. Zhang), pliaw@utk.edu (P.K. Liaw).

magnetic properties. Both investigations can shed light on the magnetic HEA design.

2. Experimental procedures

2.1. Alloy preparation

Alloy ingots of mass 50 g with nominal compositions of CoFeMn-NiAl $_x$ (x = 0.25, 0.5, 0.75, 1.0, 1.25, 1.5, and 2.0 in atomic molar ratio) were prepared by arc-melting under a high-purity argon atmosphere. The purity of the elements is higher than 99.5 wt percent. The alloys were remelted four times and flipped each time in order to improve the chemical homogeneity. The as-cast samples were annealed at 800 $^{\circ}$ C and 1000 $^{\circ}$ C for 24 h in high vacuum of about 2 \times 10 $^{-3}$ Pa, then cooled with the furnace.

2.2. Characterization

The samples about 8 mm \times 8 mm \times 2 mm were cut off from the ingots by electric-spark-wire cutting, and polished to characterize the crystal structure and microstructure. Crystal structures were identified using an X-ray diffractometer (XRD) under radiation conditions of 30 kV and 20 mA, with a Cu target and a scanning speed of 10°/min. The microstructures were examined by a ZEISS SUPRA 55 field emission scanning electron microscope (SEM) with the energy dispersive spectrometry (EDS). The detailed phase and interface structures were characterized by the JOEL 2100 transmission electron microscopy (TEM). The TEM samples were firstly electric-spark-wire cut from the ingot about Φ 3 \times 0.5 mm, then polished by sand paper to 50 μ m in thickness and followed by ion beam thinning. The magnetization curves of samples with a dimension about 4 mm \times 4 mm \times 1 mm were obtained by the instrument of a vibrating sample magnetometer. The hardness was measured by the sclerometer (HV-1000ZDT) with the load of 200 g and holding time of 15s.

3. Results

3.1. Phases and microstructures

The XRD patterns of the CoFeMnNiAl $_{\rm x}$ alloys are presented in Fig. 1. It is clear that the addition of Al makes the Al0.25 alloy maintain a simple FCC-phase structure. With the increment of the Al content, a body-centered-cubic (BCC) phase appears. Both Al0.5 and Al0.75 alloys present an FCC + BCC dual-phase structure. When the atomic ratio of Al exceeds 20%, a BCC phase dominates the alloy, and the ordered B2

phase peak comes out. The corresponding microstructures are listed in Fig. 2. From the back-scattering electron (BSE) images, two phases with an obvious composition contrast are found in Al0.5 and Al0.75 alloys, while other alloys seem to show a single phase with a polycrystalline structure. Combined with the TEM results [Fig. 3(a) and (d)], it can be determined that the BCC phase in the Al0.5 and Al0.75 alloys is exactly B2 structure, which means the Al0.5 alloy consists of an FCC matrix and a B2 second phase, while the Al0.75 alloy is composed of a B2 matrix and an FCC second phase. After annealing at 800 °C or 1000 °C for 24 h, the phases and microstructures of the alloys change greatly (Figs. 1-3). For the Al0.25 alloy, only annealing at 800 °C leads to the needle-like B2 phase to precipitate from the matrix and distribute along grain boundaries or in grains, with the volume fraction of about 16.6%. The FCC matrix is slightly rich in Fe, Co, and Al, while the B2 precipitate possesses somewhat more Ni and Mn (Table 1). For the Al0.5 alloy, annealing at both 800 °C and 1000 °C causes the needle-like B2 phase to precipitate from the FCC matrix. The content of the precipitation at 800 °C is higher and denser than that at 1000 °C, although the precipitates at 1000 °C become coarser. The volume fraction of the B2 phase at 800 °C reaches 55.7%, and its composition is rich in Al and Ni (Table 1). Similar to the Al0.5 alloy, the Al0.75 alloy annealed at 800 °C or 1000 °C still show the needle-like B2-phase precipitate from the FCC phase. However, the FCC phase becomes coarsened, and the overall content of the B2 phase decreases somewhat. The volume fractions of the B2 phase of the Al0.75 alloy at 800 $^{\circ}$ C and 1000 $^{\circ}$ C reach 71.4% and 65.1%, respectively, which means that the FCC phase also grows during annealing. Unlike the Al0.5 and Al0.75 alloys, annealing promotes the FCC-phase formation from the B2 matrix of the Al1.0 alloy. The volume fraction of the FCC phase is about 15% when annealing at 1000 °C, while 23.3% at 800 °C. As shown in our previous study, the as-cast Al1.0 alloy possesses a B2 matrix with BCC nano-particle precipitates. But from the TEM images [Fig. 3(e) and (f)] of the annealed Al1.0 alloy at 800 °C, only the B2 matrix and FCC needle-like precipitates can be seen., which means that the nano-sized BCC phase dissolved in the B2 matrix when annealing at 800 $^{\circ}\text{C}.$ The B2 and FCC phases present a coherent interface, the (110) plane of the B2 phase is parallel to the (111) plane of the FCC phase, and many twins exist in the FCC phase.

Similarly, when annealing at 800 $^{\circ}\text{C}$ for 24 h, the fine FCC phases precipitate along and around grain boundaries for Al1.25, Al1.5, and Al1.75 alloys, with the volume fractions of 11.04%, 4.37%, and 1.78%, respectively. For the Al2.0 alloy, the FCC precipitates still exist after annealing at 800 $^{\circ}\text{C}$, but its content is very small, and it can only be occasionally found. But when annealing at 1000 $^{\circ}\text{C}$, only the Al1.25 alloy has a small amount of precipitates with an uneven distribution, and other alloys maintain a polycrystalline morphology.

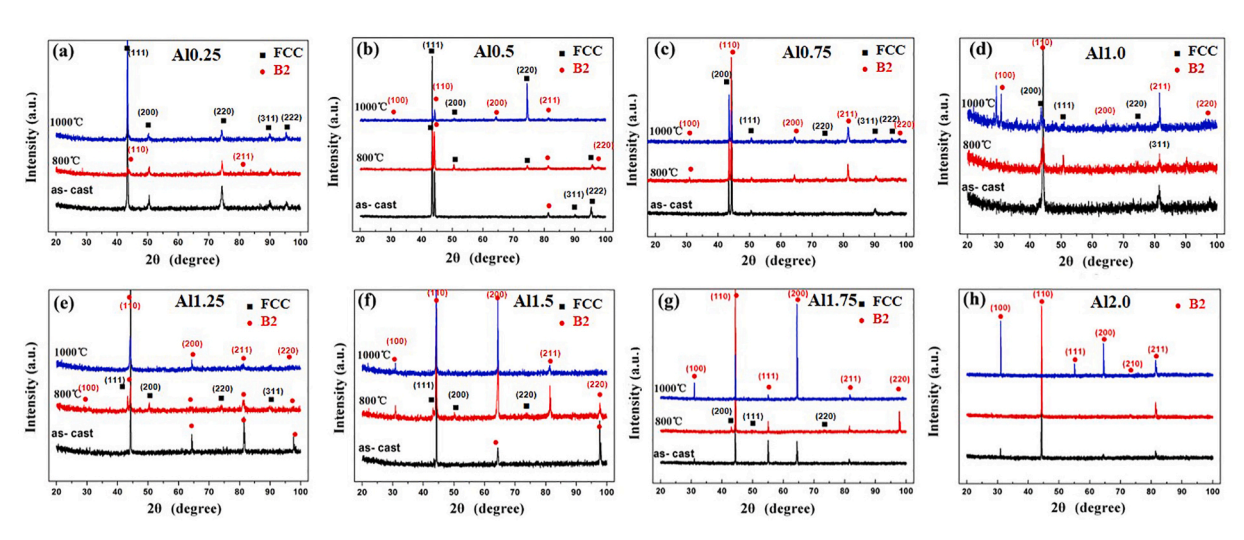


Fig. 1. The XRD patterns of the CoFeMnNiAl_x (x = 0.25, 0.5, 0.75, 1.0, 1.25, 1.5, and 2.0) alloys.

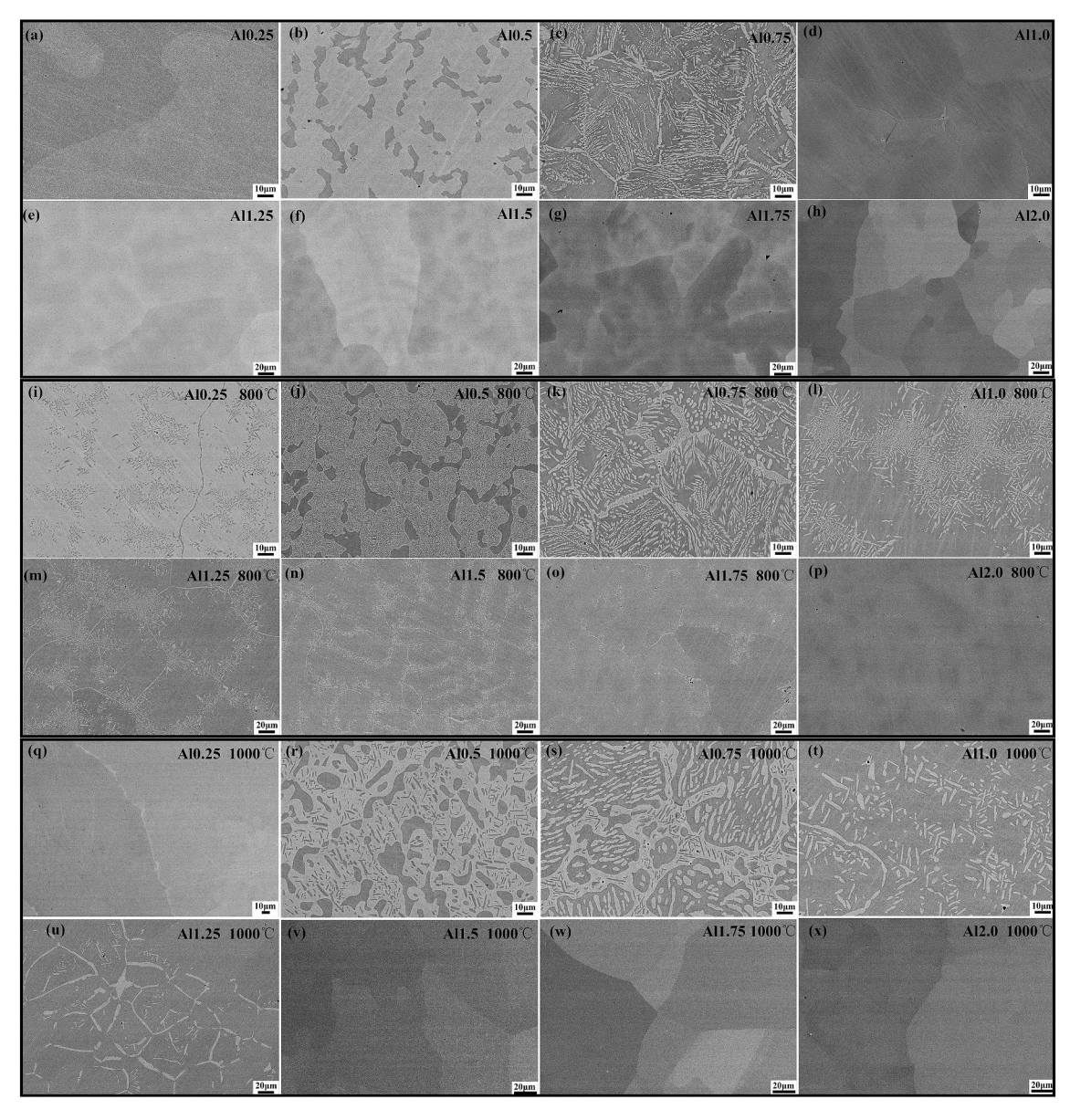


Fig. 2. The BSE images of the CoFeMnNiAl $_x$ (x = 0.25, 0.5, 0.75, 1.0, 1.25, 1.5, 1.75, and 2.0) alloys in different states.

3.2. Magnetic behavior

The room-temperature magnetic hysteresis loops of the CoFeMn-NiAlx alloys in different states are presented in Fig. 4. For the Al0.25 alloy in the as-cast state, the hysteresis loop is more like being paramagnetic with the maximum magnetization is only 13 emu/g when the magnetic field reaches 60,000 Oe. While the as-cast Al0.5-Al1.75 alloys can saturate when the magnetic field reaches 60,000 Oe. The saturation magnetization (Ms) of the as-cast alloy increases from 30.68 emu/g to 147.90 emu/g when the Al content increases from 0.5 to 1.0. Then it decreases when the Al content continues to increase from 1.0 to 2.0. However, for the as-cast Al2.0 alloy, it is not saturated when the magnetic field reaches 60,000 Oe, and its maximum magnetization is only 42.40 emu/g.

After annealing, the magnetic properties of the alloys change greatly. For the Al0.25 alloy annealed at 1000 $^{\circ}\text{C}$, the magnetism is essentially unchanged, the hysteresis loop maintains paramagnetic, while when annealed at 800 $^{\circ}\text{C}$, it turns out to be ferromagnetic with the maximum magnetization increasing to 27.52 emu/g, but it is still not saturated at the magnetic field of about 60,000 Oe. For the Al0.5 alloy, both

annealing treatments at 800 °C and 1000 °C increase the M_s value, from 30.68 emu/g to 64.14 emu/g and 55.74 emu/g. On the contrary, annealing leads the M_s of Al 0.75 and Al1.0 alloys to decrease largely, for which the M_s obtained by annealing at 800 °C is lower than that at 1000 °C. The M_s of the Al1.0 alloy can decrease from 147.90 emu/g to 113.40 emu/g (1000 °C) or 97.39 emu/g (800 °C). For Al1.25 and Al1.5 alloys, when annealing at 1000 °C, the M_s value is almost unchanged. Only annealing at 800 °C decreases the M_s . However, for Al1.75 and Al2.0 alloys, the M_s value is almost constant after annealing.

3.3. Hardness

The composition variation and annealing process bring about remarkable changes in mechanical properties of the alloys. Fig. 6 displays the hardness of the alloys affected by both annealing temperatures and Al contents. For the as-cast alloys, the hardness increases quickly with increasing the Al content, for which the volume fraction of the B2 phase increases. The alloy achieves the highest hardness of 475 HV at Al1.0. Then the hardness decreases slowly by further increasing the Al content. Annealing at 800 $^{\circ}\text{C}$ for 24 h leads Al0.25 and Al0.5 alloys to

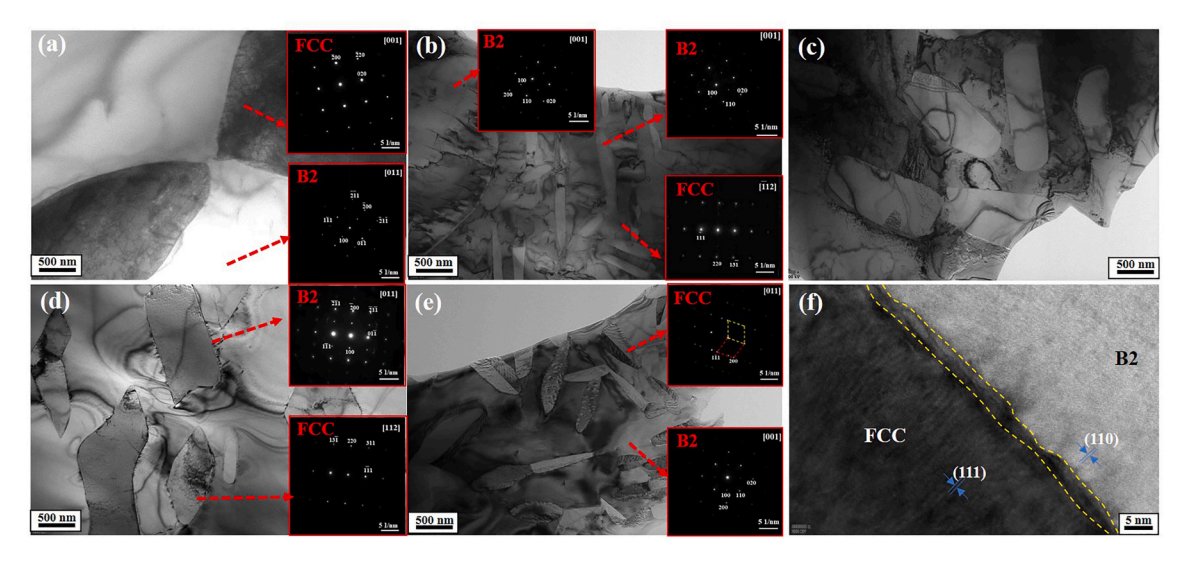


Fig. 3. The TEM images of Al0.5, Al0.75 and Al1.0 alloys (a) bright-field image with the electron-diffraction pattern from [001] axis of the matrix and electron diffraction pattern from [011] axis of the second phase of the as-cast Al0.5 alloy; (b) bright-field image with the electron-diffraction pattern from [001] axis of the needle-like phase and electron diffraction pattern from [112] axis of the matrix of the Al0.5 annealed at 800 °C; (c) bright-field image of the Al0.5 alloy annealed at 1000 °C; (d) bright-field image with the electron-diffraction pattern from [112] axis of the matrix and electron diffraction pattern from [011] axis of the precipitate of the as-cast Al0.75 alloy; (e) bright-field image with the electron diffraction pattern from [001] of the needle-like phase and electron diffraction pattern from [001] of the matrix of the Al1.0 alloy annealed at 800 °C; (d) HRTEM image of the interface between the needle phase and the matrix of the Al1.0 alloy annealed at 800 °C.

Table 1
Composition analysis of the CoFeMnNiAlx alloys in different states by EDS (at.%).

Alloy	State	Region	Crystal structure	Composition					
				Al	Mn	Fe	Со	Ni	
Al0.25	as-cast	matrix	FCC	5.35	24.07	24.04	23.71	22.83	
	800 °C	matrix	FCC	4.17	24.48	24.87	23.75	22.73	
		precipitate	B2	3.68	27.61	22.38	21/96	24.37	
A10. 5	as-cast	matrix	FCC	9.10	18.91	26.81	25.07	20.11	
		second phase	B2	17.33	23.45	13.03	18.42	27.77	
	800 °C	matrix	FCC	9.12	21.90	24.99	23.27	20.72	
		second phase	B2	18.58	22.46	10.72	18.18	30.07	
		precipitate	B2	16.68	19.56	13.52	19.40	30.85	
Al0.75	as-cast	matrix	B2	17.18	20.32	19.00	20.96	21.56	
		second phase	FCC	9.41	24.72	24.79	21.68	19.40	
	800 °C	matrix	B2	20.90	21.08	11.02	19.53	27.47	
		second phase	FCC	4.79	25.83	33.33	22.09	13.95	
		precipitate	FCC	9.62	24.24	27.15	21.37	17.62	
Al1.0	as-cast	matrix	B2+BCC	22.20	18.74	19.67	19.76	19.63	
	800 °C	matrix	B2	21.63	17.43	18.67	21.27	21.01	
		precipitate	FCC	5.86	23.82	38.11	19.80	12.40	
Al1.25	as-cast	matrix	B2	24.17	18.48	18.94	19.57	18.84	
	800 °C	matrix	B2	24.57	18.36	17.81	19.92	19.35	
		precipitate	FCC	7.85	26.63	40.17	15.97	9.38	
Al1.5	as-cast	matrix	B2	27.18	17.65	18.56	17.88	18.73	
	800 °C	matrix	B2	27.91	17.00	16.68	19.19	19.22	
		precipitate	FCC	23.54	20.39	21.44	17.80	16.83	
Al1.75	as-cast	matrix	B2	30.94	16.31	17.72	17.84	17.19	
	800 °C	matrix	B2	30.89	16.30	16.36	18.04	18.41	
		precipitate	FCC	16.47	30.08	35.39	10.85	7.21	
Al2.0	as-cast	matrix	B2	32.24	17.02	17.92	16.78	16.03	
	800 °C	matrix	B2	30.26	18.71	18.66	15.88	16.49	
		precipitate	FCC	21.92	29.98	28.18	10.76	9.16	

present an increased hardness since more B2 needle-like phases precipitate from the FCC matrix, while other alloys like Al 0.75 to Al 1.5 alloy possess a decreased hardness. The change of hardness for Al1.75 to Al2.0 alloys is not remarkable. Similarly, annealing at 1000 $^{\circ}\text{C}$ also causes the Al0.25 and Al0.5 alloys to exhibit the increased hardness. Al0.75 to Al1.25 alloys present decreased hardness, but the magnitude is not that large, compared with annealing at 800 $^{\circ}\text{C}$ because of less precipitates and the coarsening of the secondary phase. In contrast, the hardness of the Al1.5 to Al2.0 alloys increases significantly, which is due

to the homogenization of components caused by high-temperature annealing.

4. Discussions

4.1. Phase stability caused by composition and annealing

As known, HEAs are characterized by the high entropy of mixing (ΔS_{mix}), which can stabilize the solid solution and suppress the

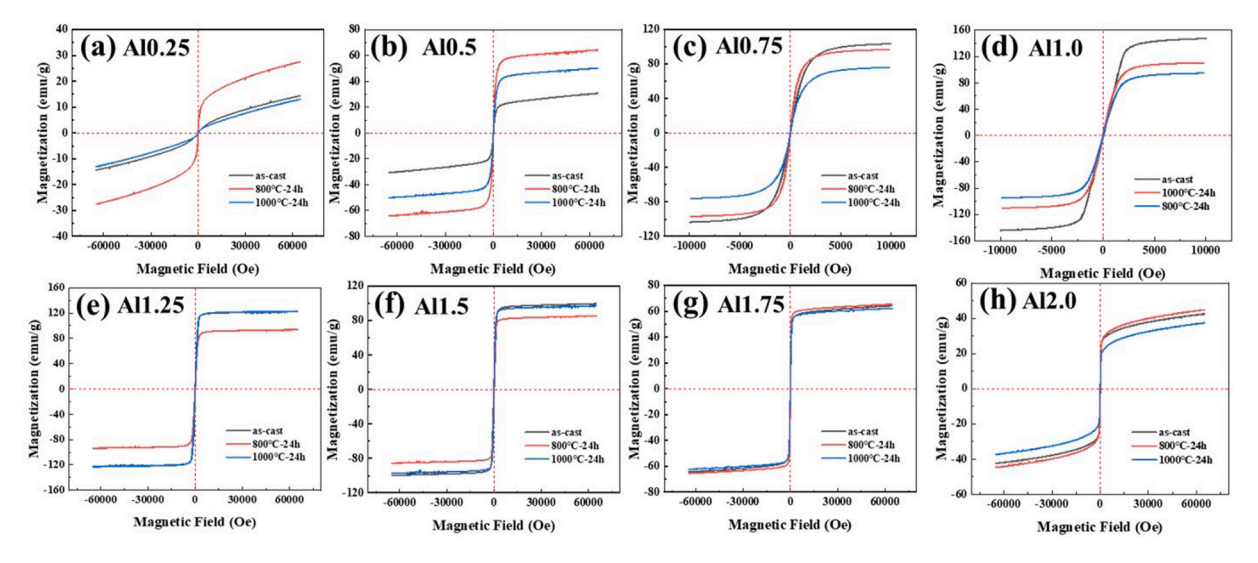


Fig. 4. The magnetic-hysteresis loops of the CoFeMnNiAl_x alloy in different states at room temperature.

formation of intermetallic compounds. However, a great amount of research shows that the high ΔS_{mix} may not always dominate the phase stability. Other empirical parameters, such as the enthalpy of mixing (ΔH_{mix}) , the atomic-size differences (δ) [24], the Ω parameter [10], the valence electron concentration (VEC) [25], the Φ -parameter [26], and the intrinsic lattice strain energy (E2/E0) [27] are proposed to guide the prediction of the solid-solution formation in multi-component alloys, the calculation methods are presented as follows:

 Ω is defined as

$$\Omega = \frac{T_{mix} \Delta S_{mix}}{|\Delta H_{mix}|} \tag{2}$$

where ΔS_{mix} , ΔH_{mix} , and T_m can be, respectively, calculated according to the following equations:

$$\Delta S_{\text{mix}} = -R \sum_{i=1}^{n} (c_i \ln c_i)$$
(3)

$$\Delta \mathbf{H}_{\text{mix}} = \sum_{i=1, i \neq j}^{n} \Omega_{ij} c_i c_j = \sum_{i=1, i \neq j}^{n} 4 c_i c_j \Delta H_{ij}^{\text{mix}}$$
(4)

$$T_{mix} = \sum_{i=1}^{n} c_i(T_m)_i \tag{5}$$

where R is the gas constant (8.314 J/K mol), c_i is the atomic percentage of the *i*th component, ΔH_{ij}^{mix} is the enthalpy of mixing of binary liquid alloys, and $(T_m)_i$ is the melting point of the *i*th component in the alloy. Ω serves as one of the key determinants for the selective formation of a solid-solution phase or an intermetallic compound.

The atomic-size differences (δ) is defined as

$$\delta = \sqrt{\sum_{i=1}^{n} c_i (1 - r_i/\bar{r})^2}$$
 (6)

where r_i is the atomic radius of the *i*th element, and \bar{r} is the average atomic radius. For the solid-solution phase with a large mutual solubility, a small atomic-size difference is needed [10].

VEC is defined as [25]

$$VEC = \sum_{i=1}^{n} c_i (VEC)_i \tag{7}$$

where VEC_i is the VEC of the *i*th element.

 Φ is defined as [26],

$$\phi = \frac{S_c - S_H}{|S_E|} \tag{8}$$

where $S_H = H_a/T_{mix}$ is the complementary entropy derived from the enthalpy $|H_a|(H_a = \Delta H_{mix})$, S_C is the configurational entropy of mixing for an ideal gas ($S_c = \Delta S_{mix}$), while S_E denotes the excessive entropy of mixing which is a function of atomic packing and atom size. The calculation of S_E is listed in Ref. [27].

Among all, Yang's and Zhang's criterion [10] is that $\Omega \ge 1.1$ and $\delta \le$ 6.6% must be satisfied to form stable disordered solid-solution phases, which means that the influence of the entropy of mixing must overshadow the enthalpy of mixing. Ye et al. 's Φ -parameter [26], which is a modification of the Ω parameter by considering the excessive entropy of mixing (S_E), needs to be greater than 20 for forming a single-phase solid solution. Applying these empirical parameters to the present alloys (Table 2 and Fig. 7), it is found that the Φ values of these alloys are all smaller than 20, implying that the alloys will not form single-phase structures. Compared with our annealing results, all the alloys are exactly multiple phases. Although the as-cast Al0.25 shows a single FCC phase in the as-cast state, it is not stable since the rapid cooling inhibits phase precipitation. During long-term annealing, elements with the negative enthalpy of mixing combine into new phases to precipitate. With the increment of the Al content, the atomic-size difference, δ , increases, which causes the larger lattice distortion, and Ω decreases, which means that the impact of the enthalpy of mixing (ΔH_{mix}) over the entropy of mixing (ΔS_{mix}) becomes more obvious. From Yang's Ω - δ criterion [10], only the Al2.0 alloy exceeds the range of $\Omega > 1.1$ and $\delta <$ 6.6% for forming disordered solid-solution phases, implying the potential to form ordered phases. By Zhang et al. 's principle [24], only Al0.25 and Al0.5 alloys locate in the disordered range, while other alloys are situated in the ordered solid-solution and intermetallic area. But the B2 phase already forms in all these alloys after annealing at 800 °C. Our results suggest that these threshold values are not universal and may fluctuate in a range. But combining the ΔH_{mix} - δ relation and the Φ value, one can determine preliminarily whether the single disordered solid-solution phase can be formed.

4.2. Magnetic-transition influence by phase structure

Magnetic materials play a key role in the modern life. One of the most important characteristics desired for either soft or hard magnetic materials is the high saturation magnetization. The saturation magnetization in this series of alloys exhibits an interesting behavior. For the

Table 2
The atomic-radius difference (δ), valence electron concentration (VEC), Ω parameter, enthalpy of mixing ($\triangle H_{mix}$), entropy of mixing ($\triangle S_{mix}$), excessive entropy of mixing (S_E), and Φ parameter of the CoFeNiMnAl_x alloys.

Alloy	δ (%)	Tm (K)	$\Delta H_{mix} (kJ/mol)$	$\Delta S_{mix}\left(J/K{\cdot}mol\right)$	Ω	VEC	Φ	Phase structure (as-cast)	Phase structure (800 °C)	Phase structure (1000 °C)
Al0.25	3.26	1661.7	-7.47	12.71	2.83	8.18	13.49	FCC	FCC + B2	FCC
Al0.5	4.29	1621.3	-10.17	13.15	2.10	7.89	8.82	FCC + B2	FCC + B2	FCC + B2
Al0.75	4.93	1585.1	-12.28	13.33	1.72	7.63	5.52	FCC + B2	FCC + B2	FCC + B2
Al1.0	5.372	1552.5	-13.92	13.38	1.49	7.40	4.42	B2+BCC	FCC + B2	FCC + B2
Al1.25	5.69	1523.0	-15.20	13.35	1.34	7.20	3.12	B2	FCC + B2	FCC + B2
Al1.5	5.91	1496.2	-16.20	13.25	1.22	7.00	2.17	B2	FCC + B2	B2
Al1.75	6.08	1471.8	-16.97	13.13	1.14	6.83	1.38	B2	FCC + B2	B2
Al2	6.20	1449.3	-17.56	12.98	1.07	6.67	0.72	B2	B2	B2

as-cast CoFeMnNiAl_x alloys, the saturation magnetization (M_s) first increases with the Al content and then decreases, and it achieves the maximum value at the Al1.0 alloy. The apparent enhancement in M_s with the Al addition can be explained by the dramatic change of the phase structure, which accordingly influences their unique electronic and magnetic structures. Since Al is a paramagnetic element, its contribution to the magnetic moment is negligible, and the significant role for adding Al is the transformation of the phase structure. During our previous study [22], it is found that the most notable change upon the addition of Al into the CoFeMnNi alloy is the formation of the B2 structure causing the shift of a Mn majority spin peak from above to below the Fermi level, which leads to a significant increase of the magnetization of CoFeMnNiAl. With increasing the Al content, the volume fraction of the B2 phase increases, and the Ms value goes up till it reaches 147.9 emu/g at the Al1.0 alloy. Similar findings are described in some references, since the conversion of the magnetic moment of Mn from being antiparallel to parallel is realized in the BCC phase [28-30]. But further increasing the Al addition has no effect on the phase structure of the matrix, and the more Al addition reduces the magnetization. This trend is similar to the CoFeNiAl_x [31] and CoFeNi(AlSi)_x [20] series alloys, for which the Al addition reduces the magnetization of the FCC-structured CoFeNi, although the Al addition causes the formation of the BCC phase. Hence, the role of Al on magnetization can't be generalized. We summarize the reported results and compared with our data in Fig. 8, it is found that the magnetization depends on the composition, the phase structure, and also the preparation technology [20,22,28,29, 31–36]. The addition of Al into the alloy, which has Mn or Cr elements with the FCC structure, may enhance the magnetization, such as the CoFeNiCrAl_x [28] and CoFeNi(MnAl)_x alloys [29].

To further understand the saturation magnetization and its dependence on the phase and composition, we performed the spin-polarized density function theory (DFT) calculations using a Vienna Ab initio Simulation Package (VASP) [37]. The calculation used a Projector Augmented Wave (PAW) method [38,39] to describe the effects of core electrons, and Perdew-Burke-Ernzerhof (PBE) [40] implementation of the Generalized Gradient Approximation (GGA) for the

exchange-correlation functional. A 108-atom FCC solid solution of FeCoNiMnAl $_x$ with x=0.32 (a unit cell lattice constant of 10.7955 Å) and a 128-atom BCC solid solution with x=1.0 (a lattice constant of 11.6176 Å) were calculated with both ferromagnetic and ferrimagnetic (with the spin of Mn antiparallel to others) configurations. It is confirmed that for x=0.32, the ferrimagnetic configuration is more stable with a lower potential energy (by 4.67 eV per unit cell), and the saturation magnetization in this case is predicted to be 40.2 emu/g. On the other hand, for x=1.0, the ferromagnetic configuration is more stable (a potential energy lower by 4.53 eV per unit cell), and its corresponding saturation magnetization is 139.5 emu/g. These results are fully consistent with the experimental data, as compared in Fig. 5(a). It should be noted that the goal of the above 0 K DFT calculation is to predict the saturation magnetization. It alone should not be used to

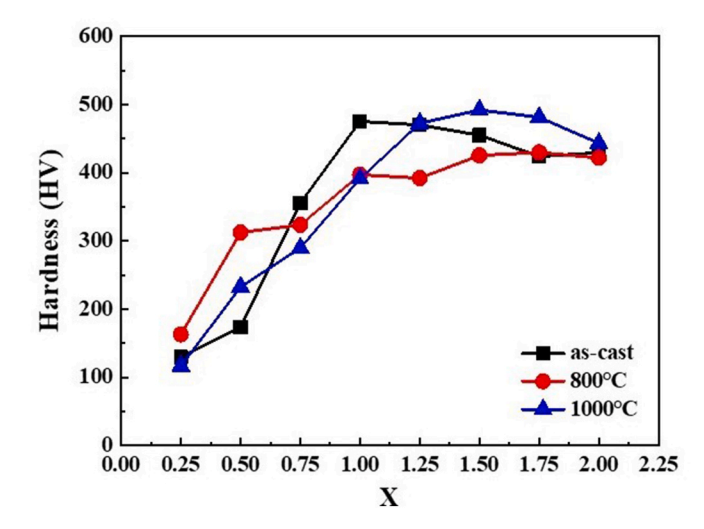


Fig. 6. The variation of hardness with the Al content of the CoFeMnNiAl $_{\rm x}$ alloys in different states.

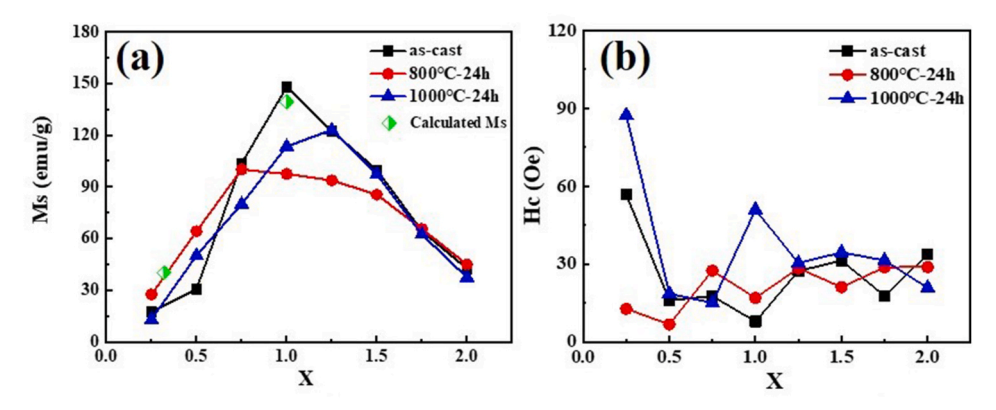


Fig. 5. The variation of saturation magnetization (Ms) and coercivity (Hc) with the Al content of the CoFeMnNiAlx alloy.

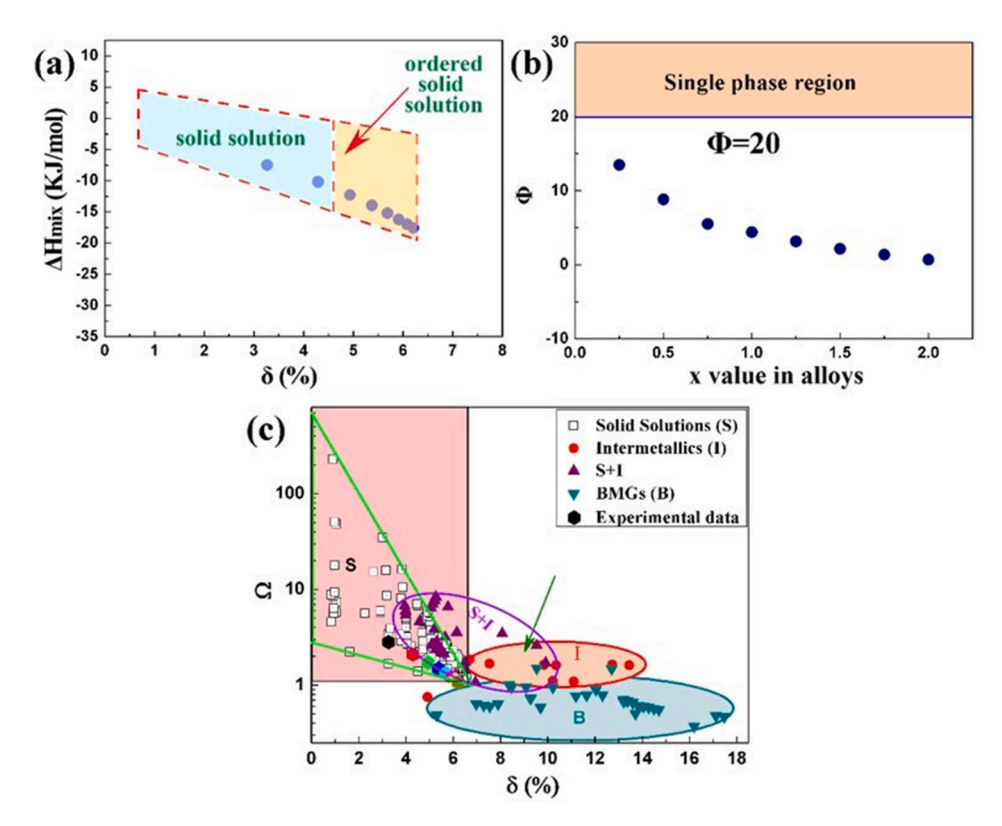


Fig. 7. (a) ΔH_{mix} -δ relation; (b) φ parameter; (c) Ω -δ relation of CoFeMnNiAl_x alloys.

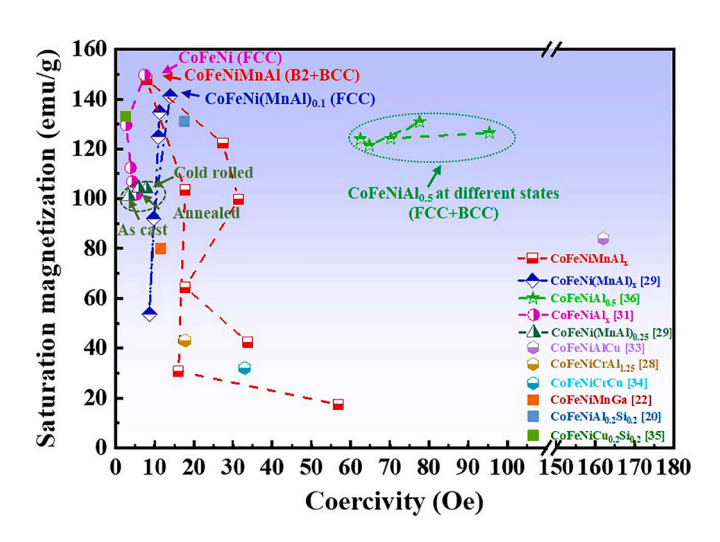


Fig. 8. The variation of Ms-Hc for different alloy systems [20,22,28,29,31–36].

predict the room temperature spontaneous magnetization as the latter requires much more involved calculations. We also note that previous DFT calculations and experimental works found that the addition of antiparallel Mn in an FCC structure can lead to a paramagnetic alloy, and a significant increment in the magnetic moment can arise from the magnetism transformation of Mn from the antiparallel to parallel state in the BCC-structure phase and the extent of the increment depends on the degree of the structural transformation [30,41,42].

Besides calculation, annealing can be another evidence for the enhanced magnetization induced by the phase transition, since for a certain alloy, annealing can't alter the composition, and it only influences the phases. The variation of the BCC-phase volume fraction and the M_{S} value are presented in Fig. 9. The M_{S} value appears to be closely related to the volume fraction of the BCC phase, and more BCC phases

lead to higher M_s values. For example, after annealing at 800 °C, the contents of the B2 phases of Al0.25 and Al0.5 alloys increase, and the M_s value rises. For Al0.75 to Al1.25 alloys, the content of the B2 phase decreases, and the M_s value goes down. By comparison, it is found that the M_s of the alloy can be estimated, using the rule of mixture:

$$M_s = M_{s,BCC}V_{BCC} + M_{s,FCC}V_{FCC} \tag{9}$$

Here, $M_{s,BCC}$ ($M_{s,FCC}$) is the M_s of the BCC (FCC) phase, and V_{BCC} (V_{FCC}) is the volume fraction of the BCC (FCC) phase. Taking the Al1.0 alloy as an example, the calculated $M_{s,FCC}$ is 50.5 emu/g, and the $M_{s,BCC}$ is 142.3 emu/g. Considering the inaccuracy in determining the volume fractions of different phases and the variations of phase components in different states, the value of $M_{s,BCC}$ is comparable to the M_s value of the as-cast alloy, which verifies the feasibility of this mixing rule.

In addition to the saturation magnetization, coercivity (H_c) , which is used as a basis for classifying soft and hard magnetic materials, is another important parameter for magnetic materials. However, unlike the saturation magnetization, coercivity presents a complex trend, since coercivity is influenced by microstructures, such as dislocations, grain boundaries, phase-boundary, precipitates, as well as the constituent components. The relationship between the coercivity and the precipitate is described as follows [43]:

$$H_c \propto \frac{\delta_\omega K_1}{M_s \mu_0 r} v_f^{2/3} \tag{10}$$

where H_c is the coercivity, M_s the saturation magnetization, K_1 the magnetocrystalline anisotropy, δ_ω the wall thickness, μ_0 the permeability of the vacuum, \bar{r} the average radius of the particles, and V_f , their volume fraction. For the Al0.25 alloy, the saturation magnetization is the most important factor that influences the coercivity, and the coercivity is inversely proportional to the saturation magnetization. For Al0.5, Al0.75, and Al1.0 alloys, due to the very high-volume fraction of the precipitates, the coercivity is affected not only by the saturation magnetization but also by the precipitate. Taking the Al1.0 alloy as an

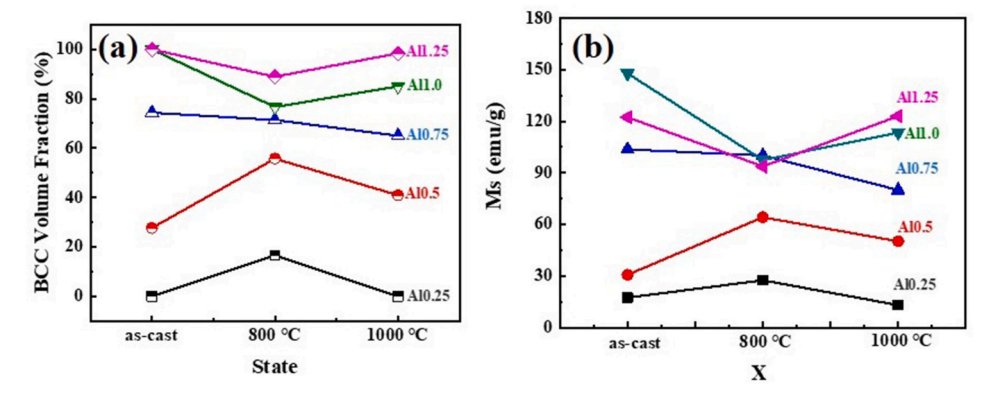


Fig. 9. The variation of the BCC-phase volume fraction and the Ms value of the Al CoFeMnNiAl_x (x = 0.25, 0.5, 0.75, 1.0, and 1.25) alloys in different states.

example, the as-cast alloy presents nearly single phases with the polycrystalline structure, and its M_s value is the highest. Hence, the H_c is the lowest (Fig. 5(b)). After annealing, the M_s decreases, and the needle-like FCC precipitates with lower M_s values appear (Fig. 2). The smaller radius and the higher volume fraction of the precipitates significantly increase the H_c value. Since the factors that affect H_c are very complex, other factors, including the grain size, the magnetocrystalline anisotropy, the magnetic domain wall thickness, and the permeability of vacuum, etc. should be considered.

5. Conclusions

To summarize, we have experimentally and theoretically studied the phase stability of CoFeMnNiA $_{\rm lx}$ alloys. The structure-induced magnetization transition is thoroughly explored and explained by DFT calculations. The present research offers a pathway to the fundamental design and development of structural and functional HEAs. The pertinent results are summarized as follows.

- (1) The Al addition leads to the phase transition from the FCC to B2 structures for CoFeMnNiA_{lx} alloys, which significantly enhances the magnetization. The magnetic transition is verified by the *ab initio* simulation, which conforms the turning of antiparallel order to parallel order caused by phase transition. However, further increasing the aluminum content in the B2-structured alloy weakens the magnetization, causing a lower M_s value.
- (2) The phase stability of the CoFeMnNiAl $_x$ alloy is thoroughly studied by long-time annealing. Long-time annealing can cause the needle B2 phase to be precipitated from the FCC phase (x \leq 0.5) or FCC phase to be precipitated from the B2 phase (x \geq 0.75). By comparison, the existing empirical criteria used to predict the phase formation are not universal, but combining the ΔH_{mix} δ relation and the Φ value, whether the single disordered solid-solution phase is formed can be preliminarily predicted.
- (3) The magnetization is significantly influenced by the volume fraction of the B2 phase. The appearance of the needle-like FCC phase continuously precipitated from the B2 matrix for Al0.75-Al1.75 alloys after annealing decreases the $M_{\rm s}$ value.

CRediT authorship contribution statement

Tingting Zuo: Conceptualization, Data curation, Formal analysis, Investigation, Writing – original draft, Resources. **Yongqiang Cheng:** Software, Formal analysis. **Peiyong Chen:** Formal analysis, Methodology. **Zhaoshun Gao:** Writing – review & editing. **Yong Zhang:** Conceptualization, Supervision, Writing – review & editing. **Peter K. Liaw:** Funding acquisition, Supervision, Writing – review & editing.

Declaration of competing interest

The authors declare that they have no known competing financial interests or personal relationships that could have appeared to influence the work reported in this paper.

Acknowledgement

The present work is supported by the National Natural Science Foundation of China (grant number 51901221). P. K. Liaw very much appreciates the supports from (1) the National Science Foundation (DMR-1611180 and 1809640) with program directors, Drs. J. Yang, G. Shiflet, and D. Farkas and (2) the US Army Research Office (W911NF-13–1-0438 and W911NF-19–2-0049) with program managers, Drs. M.P. Bakas, S.N. Mathaudhu, and D.M. Stepp. Y.Q. Cheng was supported in part by the US Department of Energy, Office of Basic Energy Sciences, Division of Scientific User Facilities. The computing resources were made available through the VirtuES project, funded by the Laboratory Directed Research and Development program and Compute and Data Environment for Science (CADES) at ORNL.

References

- E.P. George, D. Raabe, R.O. Ritchie, High-entropy alloys, Nat. Rev. Mater. 4 (2019) 515–534.
- [2] Q. Ding, Y. Zhang, X. Chen, X. Fu, D. Chen, S. Chen, L. Gu, F. Wei, H. Bei, Y. Gao, M. Wen, J. Li, Z. Zhang, T. Zhu, R.O. Ritchie, Q. Yu, Tuning element distribution, structure and properties by composition in high-entropy alloys, Nature 574 (2019) 223–227.
- [3] D.B. Miracle, High entropy alloys as a bold step forward in alloy development, Nat. Commun. 10 (2019) 1805.
- [4] C. Niu, C.R. LaRosa, J. Miao, M.J. Mills, M. Ghazisaeidi, Magnetically-driven phase transformation strengthening in high entropy alloys, Nat. Commun. 9 (2018) 1363.
- [5] E.P. George, W.A. Curtin, C.C. Tasan, High entropy alloys: a focused review of mechanical properties and deformation mechanisms, Acta Mater. 188 (2020) 435–474.
- [6] D.B. Miracle, O.N. Senkov, A critical review of high entropy alloys and related concepts, Acta Mater. 122 (2017) 448–511.
- [7] B. Cantor, I.T.H. Chang, P. Knight, A.J.B. Vincent, Microstructural development in equiatomic multicomponent alloys, Mater. Sci. Eng., A 375–377 (2004) 213–218.
- [8] J.W. Yeh, S.K. Chen, S.J. Lin, J.Y. Gan, T.S. Chin, T.T. Shun, C.H. Tsau, S.Y. Chang, Nanostructured high-entropy alloys with multiple principal elements: novel alloy design concepts and outcomes. Adv. Eng. Mater. 6 (2004) 299–303.
- [9] Y. Zhang, T.T. Zuo, Z. Tang, M.C. Gao, K.A. Dahmen, P.K. Liaw, Z.P. Lu, Microstructures and properties of high-entropy alloys, Prog. Mater. Sci. 61 (2014) 1–93.
- [10] X. Yang, Y. Zhang, Prediction of high-entropy stabilized solid-solution in multicomponent alloys. Mater. Chem. Phys. 132 (2) (2012) 233–238.
- [11] X. Gao, Y. Lu, B. Zhang, N. Liang, G. Wu, G. Sha, J. Liu, Y. Zhao, Microstructural origins of high strength and high ductility in an AlCoCrFeNi2.1 eutectic highentropy alloy, Acta Mater. 141 (2017) 59–66.
- [12] L.L. Xiao, Z.Q. Zheng, S.W. Guo, P. Huang, F. Wang, Ultra-strong nanostructured CrMnFeCoNi high entropy alloys, Mater. Des. 194 (2020) 108895.
- [13] G. Bernd, A fracture-resistant high-entropy alloy for cryogenic applications, Science (2014) 6201.

- [14] M.A. Hemphill, T. Yuan, G.Y. Wang, J.W. Yeh, C.W. Tsai, A. Chuang, P.K. Liaw, Fatigue behavior of Al0.5CoCrCuFeNi high entropy alloys, Acta Mater. 60 (2012) 5723–5734
- [15] K. Liu, S.S. Nene, M. Frank, S. Sinha, R.S. Mishra, Extremely high fatigue resistance in an ultrafine grained high entropy alloy, Appl. Mater. Today 15 (2019) 525–530.
- [16] S.W. Wu, G. Wang, Q. Wang, Y.D. Jia, J. Yi, Q.J. Zhai, J.B. Liu, B.A. Sun, H.J. Chu, J. Shen, P.K. Liaw, C.T. Liu, T.Y. Zhang, Enhancement of strength-ductility tradeoff in a high-entropy alloy through a heterogeneous structure, Acta Mater. 165 (2019) 444–458.
- [17] H. Jiang, D. Qiao, Y. Lu, Z. Ren, Z. Cao, T. Wang, T. Li, Direct solidification of bulk ultrafine-microstructure eutectic high-entropy alloys with outstanding thermal stability, Scripta Mater. 165 (2019) 145–149.
- [18] Y. Shi, L. Collins, R. Feng, C. Zhang, N. Balke, P.K. Liaw, B. Yang, Homogenization of AlxCoCrFeNi high-entropy alloys with improved corrosion resistance, Corrosion Sci. 133 (2018) 120–131.
- [19] P. Li, A. Wang, C.T. Liu, A ductile high entropy alloy with attractive magnetic properties, J. Alloys Compd. (2017) 55–60.
- [20] Y. Zhang, T. Zuo, Y. Cheng, P.K. Liaw, High-entropy alloys with high saturation magnetization, electrical resistivity and malleability, Sci. Rep. 3 (2013) 1455.
- [21] K.X. Zhou, B.R. Sun, G.Y. Liu, X.W. Li, S.W. Xin, P.K. Liaw, T.D. Shen, FeCoNiAlSi high entropy alloys with exceptional fundamental and application-oriented magnetism, Intermetallics 122 (2020) 106801.
- [22] T. Zuo, M.C. Gao, L. Ouyang, X. Yang, Y. Cheng, R. Feng, S. Chen, P.K. Liaw, J. A. Hawk, Y. Zhang, Tailoring magnetic behavior of CoFeMnNiX (X = Al, Cr, Ga, and Sn) high entropy alloys by metal doping, Acta Mater. 130 (2017) 10–18.
- [23] C. Ng, S. Guo, J. Luan, Q. Wang, J. Lu, S. Shi, C.T. Liu, Phase stability and tensile properties of Co-free Al0.5CrCuFeNi₂ high-entropy alloys, J. Alloys Compd. 584 (2014) 530–537. 0.
- [24] Y. Zhang, Y.J. Zhou, J.P. Lin, G.L. Chen, P.K. Liaw, Solid-solution phase formation rules for multi-component alloys, Adv. Eng. Mater. 10 (2008) 534–538.
- [25] S. Guo, C. Ng, J. Lu, C.T. Liu, Effect of valence electron concentration on stability of fcc or bcc phase in high entropy alloys, J. Appl. Phys. 109 (2011) 103505.
- [26] Y.F. Ye, Q. Wang, J. Lu, C.T. Liu, Y. Yang, Design of high entropy alloys: a single-parameter thermodynamic rule, Scripta Mater. 104 (2015) 53–55.
- [27] Z. Wang, W. Qiu, Y. Yang, C.T. Liu, Atomic-size and lattice-distortion effects in newly developed high-entropy alloys with multiple principal elements, Intermetallics 64 (2015) 63–69.
- [28] Y.F. Kao, S.K. Chen, T.J. Chen, P.C. Chu, J.W. Yeh, S.J. Lin, Electrical, magnetic, and Hall properties of Al_xCoCrFeNi high-entropy alloys, J. Alloys Compd. 509 (2011) 1607–1614.

- [29] Z. Li, G. Bai, X. Liu, S. Bandaru, Z. Wu, X. Zhang, M. Yan, H. Xu, Tuning phase constitution and magnetic properties by composition in FeCoNiAlMn high-entropy alloys, J. Alloys Compd. 845 (2020).
- [30] B. Zhang, Y. Duan, H. Zhang, S. Huang, G. Ma, T. Wang, X. Dong, N. Jia, Magnetic transformation of Mn from anti-ferromagnetism to ferromagnetism in FeCoNiZMnx (Z = Si, Al, Sn, Ge) high entropy alloys, J. Mater. Sci. Technol. 68 (2021) 124–131.
- [31] T.T. Zuo, R.B. Li, X.J. Ren, Y. Zhang, Effects of Al and Si addition on the structure and properties of CoFeNi equal atomic ratio alloy, J. Magn. Magn Mater. 371 (2014) 60–68.
- [32] S. Huang, W. Li, X. Li, S. Schönecker, L. Bergqvist, E. Holmström, L.K. Varga, L. Vitos, Mechanism of magnetic transition in FeCrCoNi-based high entropy alloys, Mater. Des. 103 (2016) 71–74.
- [33] R. Kulkarni, B.S. Murty, V. Srinivas, Study of microstructure and magnetic properties of AlNiCo(CuFe) high entropy alloy, J. Alloys Compd. 746 (2018) 194–199
- [34] V. Chaudhary, V. Soni, B. Gwalani, R.V. Ramanujan, R. Banerjee, Influence of non-magnetic Cu on enhancing the low temperature magnetic properties and Curie temperature of FeCoNiCrCu(x) high entropy alloys, Scripta Mater. 182 (2020) 90-103
- [35] C. Chen, H. Zhang, Y. Fan, W. Zhang, R. Wei, T. Wang, T. Zhang, F. Li, A novel ultrafine-grained high entropy alloy with excellent combination of mechanical and soft magnetic properties, J. Magn. Magn Mater. 502 (2020) 166513.
- [36] J. Xu, J.Y. Zhang, Y.Q. Wang, P. Zhang, J. Kuang, G. Liu, G.J. Zhang, J. Sun, Annealing-dependent microstructure, magnetic and mechanical properties of highentropy FeCoNiAl0.5 alloy, Mater. Sci. Eng., A 776 (2020) 139003.
- [37] G. Kresse, J. Furthmüller, Efficient iterative schemes for ab initio total-energy calculations using a plane-wave basis set, Phys. Rev. B Condens. Matter 54 (1996) 11169–11186.
- [38] P.E. Blöchl, Projector augmented-wave method, Phys. Rev. B Condens. Matter 50 (1994) 17953–17979.
- [39] G. Kresse, D. Joubert, From ultrasoft pseudopotentials to the projector augmentedwave method, Phys. Rev. B Condens. Matter 59 (1999) 1758–1775.
- [40] J.P. Perdew, K. Burke, M. Ernzerhof, Generalized gradient approximation made simple, Phys. Rev. Lett. 77 (18) (1996) 3865–3868.
- [41] C. Zhao, J. Li, Y. Liu, X. Ma, Y. Jin, W.Y. Wang, H. Kou, J. Wang, Optimizing mechanical and magnetic properties of AlCoCrFeNi high-entropy alloy via FCC to BCC phase transformation, J. Mater. Sci. Technol. 86 (2021) 117–126.
- [42] S. Huang, E. Holmström, O. Eriksson, L. Vitos, Mapping the magnetic transition temperatures for medium- and high-entropy alloys, Intermetallics 95 (2018) 80–84.
- [43] J.M.D. Coey, Magnetism and Magnetic Materials, Cambridge University Press, Cambridge, UK, 2009.